

Symmetric interpolatory framelets and their erasure recovery properties *

O. Amrani², A. Z. Averbuch¹, T. Cohen¹ and V. A. Zheludev¹

¹School of Computer Science, Tel Aviv University, Tel Aviv 69978, Israel

e-mail:{amir1,tamircoh,zhel}@post.tau.ac.il

²Department of Electrical Engineering - Systems, School of Electrical Engineering

Faculty of Engineering, Tel Aviv University, Tel Aviv 69978, Israel

ofer@neg.tau.ac.il

Abstract

A new class of wavelet-type frames in signal space that uses (anti)symmetric waveforms is presented. The construction employs interpolatory filters with rational transfer functions. These filters have linear phase. They are amenable either to fast cascading or parallel recursive implementation. Robust error recovery algorithms are developed by utilizing the redundancy inherent in frame expansions. Experimental results recover images when (as much as) 60% of the expansion coefficients are either lost or corrupted. The proposed approach inflates the size of the image through framelet expansion and multilevel decomposition thus providing redundant representation of the image. Finally, the frame-based error recovery algorithm is compared with a classical coding approach.

1 Introduction

Frames provide redundant representations of signals. This redundancy enables to exploit frame expansion as a tool for recovery of erasures, which may occur while a multimedia signal is transmitted through a lossy channel ([13, 21]). An important class of frames, which is especially feasible for signal processing, is the class of frames generated by oversampled perfect reconstruction filter banks (OPRFB) [7, 16]. Actually, the frame transforms of multimedia signals provided by filter bank can be interpreted as joint source-channel encoding for lossy channels, which is resilient to quantization noise and erasures. This approach was developed in [10, 26, 15, 25]. Orthogonal tree-structured OPRFB were presented

*The research was partially supported by STRIMM Consortium (2004-2005) administrated by the Ministry of Trade of Israel.

in [26] as a tool for the error correction. The frames were formed by two-channel non-decimated filter banks. In [25] cosine-modulated OPRFBs generate frames for the error correction.

Pursuing a similar approach to the joint source-channel encoding, we propose to use for this purpose recently constructed wavelet frames (framelets), which are generated by three-channel OPRFBs with the downsampling factor of 2 [4]. Such frames provide a minimal redundancy. We present a collection of such filter banks based on Butterworth filters. The frames combine high computational efficiency of the wavelet pyramid scheme with the power and flexibility of redundant representations. The framelets originating from the presented filter banks possess a combination of properties that are valuable for signal and image processing: symmetry, interpolation, fair time-domain localization, flat spectra and any number of vanishing moments. The simplicity and low complexity involved in the decomposition and reconstruction of the designed frames, give rise to efficient joint source-channel coding and decoding. These properties promise good error recovery capabilities. Results of our experiments with erasure recovery in multimedia images confirm this claim. It is shown by means of simulations that these framelets can effectively recover from random losses that are close to the theoretical limit.

Unlike most schemes of the construction of wavelets and wavelet frames, we use infinite impulse response (IIR) filters with rational transfer functions. Consequently, the corresponding waveforms do not have compact support. But this fact should hardly be counted as a drawback because of the exponential decay of the waveforms as the argument grows. As for the implementation, it can be carried out in a fast recursive mode. On the other hand, usage of IIR filters enables to achieve a combination of properties, which are impossible to get with finite impulse response (FIR) filters. For example, it was proved in [31] that only one tight frame can be designed using three-channel interpolatory linear phase FIR filter banks with downsampling factor of 2. The framelets of this single frame are piece-wise linear. One of them has two vanishing moments while the other has only one. We cite this example in Section 2 (Eq. (2.16)). A hard problem in the construction of framelets that are based on FIR filter banks is combining symmetry with a sufficient number of vanishing moments. Currently, only (anti)symmetric framelets with 3 vanishing moments are designed [19, 33].

Note that wavelet constructions that are based on filter banks with rational transfer functions were originally introduced in [18]. In particular, non-symmetric wavelets that are based on causal Butterworth filters were presented in [18]. Petukhov [29] designed a family of symmetric wavelets with rational symbols and applied them to video compression [8]. Another collection of biorthogonal symmetric wavelets with rational symbols, which is based on properties of continuous and discrete splines, was presented in [2, 1] and successfully applied to image compression [3].

A parameterized family of linear phase low-pass filters with rational transfer functions, which admits formation of tight frames with two generating (anti)symmetric framelets having two vanishing moments

was presented in [30]. Later, a collection of wavelet frames has been designed ([4]), which is used in this paper. We outline briefly this construction in Section 2.

Conventional methods for protecting data are well developed both in theory and in practice. Block and convolutional codes are considered to be very efficient classes of channel codes. They are widely used in wireless and wire-line channels such as the internet. However, these codes, and other conventional methods, do not generally take into account the inner structure of the transmitted (multimedia) signal. Rather, it is assumed that every information bit is equally significant, and hence it has to be equally protected. Multimedia information usually undergoes some transform (e.g. DCT, FFT or wavelet) followed by quantization and lossless compression (entropy coding). The last two operations constitute source coding. The resulting binary sequence (which assumed to be white noise) typically contains bits with unequal significance, which must be protected accordingly. Due to this inhomogeneity, direct application of channel coding methods to audio-visual information, is not optimal; it may significantly increase the transmission length if the (equal) error correction code is chosen according to the most vulnerable data. Hence, it is desired to design error correction codes that dynamically allocate more bits to more important information. Such codes are known as unequal error protection codes. Due to the growing importance in rich multimedia data transmission, unequal error protection methods have attracted research efforts, see e.g. [23] and the references therein. For example, ([22, 23]) irregular repeat accumulate (IRA) codes [20] of different rates are designed and applied for scalable image transmission over binary symmetric channel (BSC). The different rates are obtained by puncturing the parity bits of a mother IRA code, which uses a symmetric encoder.

The main results of this paper can be summarized as follows:

- Design of new families of symmetric wavelet frames based on oversampled perfect reconstruction filter banks with rational transfer functions.
- Usage of these frames as a base for the source-channel coding scheme aimed for the recovery of erasures in the transmitted multimedia images.

The paper has the following structure. In Section 2 we describe the construction of symmetric frames in signal space associated with low-pass filters with rational transfer functions. In Section 3 we present error recovery algorithms that utilize the redundancy inherent in frame expansions that were designed in Section 2. The Griesmer bound is invoked in Eq. 4.2 for comparing between the framelet based error-recovery algorithm and a classical coding approach. Finally, Section 5 provides some simulation results.

2 Design of frames

In this section, we briefly describe construction of wavelet-type frames in the signal space using linear phase filter banks that comprise interpolatory filters related to the Butterworth filters. The constructions are based on the results in [4]. More details are given there.

2.1 Filter banks

We call the sequences $\mathbf{x} \triangleq \{x_k\}$, $k \in \mathbb{Z}$, which belong to the space l_1 , (and, consequently, to l_2) discrete-time signals. The z -transform of a signal \mathbf{x} is defined as $X(z) \triangleq \sum_{k \in \mathbb{Z}} z^{-k} x_k$.

Digital filtering of a signal x_n is $y_n = \sum_{k \in \mathbb{Z}} f_{n-k} x_k$. The sequence $\{f_n\}$ is called the impulse response of the filter \mathbf{f} . Its z -transform $F(z) \triangleq \sum_{n \in \mathbb{Z}} z^{-n} f_n$ is the transfer function of the filter. Usually, a filter is designated by its transfer function $F(z)$. The function $\hat{F}(\omega) = F(e^{j\omega})$ is called the frequency response of the digital filter.

In this paper, we consider 3-channel filter banks, where each contains one low-pass, one band-pass and one high-pass filters and the downsampling factor is $N = 2$. Their transfer functions are rational functions, which do not have poles on the unit circle $|z| = 1$. Thus, the impulse responses belong to the signal space. We denote the analysis and synthesis low-pass filters by $\tilde{H}(z)$ and $H(z)$, respectively, and the high-pass filters are denoted by $\tilde{G}^r(z)$ and $G^r(z)$, $r = 1, 2$. We denote by \mathbf{s}^1 , $\mathbf{d}^{r,1}$, $r = 1, 2$, the output signals from the downsampled analysis filter bank. These signals are the input for the upsampled synthesis filter bank. Then, the analysis and synthesis formulas become:

$$s_l^1 = 2 \sum_{n \in \mathbb{Z}} \tilde{h}_{n-2l} x_n \Leftrightarrow S^1(z^2) = \tilde{H}(1/z)X(z) + \tilde{H}(-1/z)X(-z), \quad (2.1)$$

$$d_l^{r,1} = 2 \sum_{n \in \mathbb{Z}} \tilde{g}_{n-2l}^r x_n \Leftrightarrow D^{r,1}(z^2) = \tilde{G}^r(1/z)X(z) + \tilde{G}^r(-1/z)X(-z), \quad r = 1, 2, \quad (2.2)$$

$$\hat{x}_l = \sum_{n \in \mathbb{Z}} h_{l-2n} s_n^1 + \sum_{r=1}^2 \sum_{n \in \mathbb{Z}} g_{l-2n}^{r,1} d_n^{r,1} \Leftrightarrow \hat{X}(z) = H(z)S^1(z^2) + \sum_{r=1}^2 G^{r,1}(z)d^r(z^2). \quad (2.3)$$

Polyphase representation of filtering: The functions

$$F_e(z) \triangleq \sum_{k \in \mathbb{Z}} z^{-k} f_{2k}, \quad F_o(z) \triangleq \sum_{k \in \mathbb{Z}} z^{-k} f_{2k+1}, \quad E(z) \triangleq \sum_{k \in \mathbb{Z}} z^{-k} x_{2k}, \quad O(z) \triangleq \sum_{k \in \mathbb{Z}} z^{-k} x_{2k+1}$$

are the polyphase components of $F(z)$ and $X(z)$, respectively.

The analysis $\tilde{\mathbf{P}}(z)$ and the synthesis $\mathbf{P}(z)$ *polyphase matrices*, respectively, are:

$$\tilde{\mathbf{P}}(z) \triangleq \begin{pmatrix} \tilde{H}_e(z) & \tilde{H}_o(z) \\ \tilde{G}_e^1(z) & \tilde{G}_o^1(z) \\ \tilde{G}_e^2(z) & \tilde{G}_o^2(z) \end{pmatrix}, \quad \mathbf{P}(z) \triangleq \begin{pmatrix} H_e(z) & G_e^1(z) & G_e^2(z) \\ H_o(z) & G_o^1(z) & G_o^2(z) \end{pmatrix}.$$

Then,

$$\begin{pmatrix} S^1(z) \\ D^{1,1}(z) \\ D^{2,1}(z) \end{pmatrix} = 2\tilde{\mathbf{P}}(1/z) \cdot \begin{pmatrix} E(z) \\ O(z) \end{pmatrix}, \quad \begin{pmatrix} \hat{E}(z) \\ \hat{O}(z) \end{pmatrix} = \mathbf{P}(z) \cdot \begin{pmatrix} S^1(z) \\ D^{1,1}(z) \\ D^{2,1}(z) \end{pmatrix}.$$

Here, $\hat{E}(z)$ and $\hat{O}(z)$ are the z -transforms of the even and odd components of the output signal $\hat{\mathbf{x}}$, respectively. If the signal $\hat{\mathbf{x}} = \mathbf{x}$ then the analysis and synthesis filter banks form a perfect reconstruction filter bank. Analytically, this property is expressed via the polyphase matrices as

$$\mathbf{P}(z) \cdot \tilde{\mathbf{P}}(1/z) = \frac{1}{2}\mathbf{I}, \quad (2.4)$$

where \mathbf{I} is the 2×2 identity matrix. Thus, the synthesis polyphase matrix must be a left inverse of the analysis matrix (up to factor $1/2$). Obviously, if such a matrix exists, it is not unique.

2.2 Frames

Definition 2.1 A system $\tilde{\Phi} \triangleq \{\tilde{\phi}_j\}_{j \in \mathbb{Z}}$ of signals forms a frame of the signal space if there exist positive constants A and B such that for any signal $\mathbf{x} = \{x_l\}_{l \in \mathbb{Z}}$

$$A\|\mathbf{x}\|^2 \leq \sum_{j \in \mathbb{Z}} |\langle \mathbf{x}, \tilde{\phi}_j \rangle|^2 \leq B\|\mathbf{x}\|^2.$$

If the frame bounds A and B are equal to each other then the frame is said to be tight.

If the system $\tilde{\Phi}$ is a frame then there exists another frame $\Phi \triangleq \{\phi_i\}_{i \in \mathbb{Z}}$ of the signals space such that any signal \mathbf{x} can be expanded into the sum $\mathbf{x} = \sum_{i \in \mathbb{Z}} \langle \mathbf{x}, \tilde{\phi}_i \rangle \phi_i$. The frames $\tilde{\Phi}$ and Φ can be interchanged. Together they form the so-called bi-frame. If the frame is tight then Φ can be chosen as $\Phi = c\tilde{\Phi}$.

Assume we have analysis $\tilde{H}(z)$, $\tilde{G}^1(z)$ $\tilde{G}^2(z)$ and synthesis $H(z)$, $G^1(z)$ $G^2(z)$ filter banks such that the impulse responses of the filters belong to the signal space. We define the discrete-time framelets of the first decomposition scale to be the impulse responses of the filters:

$$\tilde{\varphi}^1 \triangleq \{\tilde{\varphi}^1(n) \triangleq 2\tilde{h}(n)\}, \quad \tilde{\psi}^{r,1} \triangleq \{\tilde{\psi}^{r,1}(n) \triangleq 2\tilde{g}^r(n)\}, \quad \varphi^1 \triangleq \{\varphi^1(n) \triangleq 2h(n)\}, \quad \psi^{r,1} \triangleq \{\psi^{r,1}(n) \triangleq 2g^r(n)\}.$$

Here, $r = 1, 2$, $n \in \mathbb{Z}$. Then, the analysis and synthesis Eqs. (2.1) and (2.2) can be presented in the following way:

$$s_l^1 = \langle \mathbf{x}, \tilde{\varphi}^1(\cdot - 2l) \rangle, \quad d_l^{r,1} = \langle \mathbf{x}, \tilde{\psi}^{r,1}(\cdot - 2l) \rangle, \quad r = 1, 2, l \in \mathbb{Z},$$

$$\hat{\mathbf{x}} = \frac{1}{2} \sum_{l \in \mathbb{Z}} s_l^1 \varphi^1(\cdot - 2l) + \frac{1}{2} \sum_{r=1}^2 \sum_{l \in \mathbb{Z}} d_l^{r,1} \psi^{r,1}(\cdot - 2l).$$

If the given set of filters forms a perfect reconstruction filter bank then we have

$$\mathbf{x} = \frac{1}{2} \sum_{l \in \mathbb{Z}} \langle \mathbf{x}, \tilde{\varphi}^1(\cdot - 2l) \rangle \varphi^1(\cdot - 2l) + \frac{1}{2} \sum_{r=1}^2 \sum_{l \in \mathbb{Z}} \langle \mathbf{x}, \tilde{\psi}^{r,1}(\cdot - 2l) \rangle \psi^{r,1}(\cdot - 2l). \quad (2.5)$$

Thus, if the condition (2.4) is satisfied then the set of two-sample shifts of the signals $\tilde{\varphi}^1$, $\tilde{\psi}^{r,1}$, and φ^1 , $\psi^{r,1}$, $r = 1, 2$, form a bi-frame of the signal space. If $\mathbf{P}(z) = c\tilde{\mathbf{P}}^T(z)$ then the signals φ^1 and $\psi^{r,1}$, $r = 1, 2$, generate a tight frame.

Definition 2.2 *It is said that a discrete-time framelet ψ has m vanishing moments if $\sum_{k \in \mathbb{Z}} \psi(k) k^r = 0$, $k = 0, \dots, m - 1$.*

If the framelet ψ is defined as the impulse response of a high-pass filter $G(z)$ then the number of its vanishing moments is equal to the multiplicity of zero of the function $G(z)$ at $z = 1$.

Multiscale frame transforms The iterated application of the analysis filter bank to the signal $\mathbf{s}^1 = \{s_k^1\}$ produces the following three signals assuming $r = 1, 2$:

$$\begin{aligned} s_l^2 &= \sum_{n \in \mathbb{Z}} \tilde{h}_{n-2l} s_n^1 = \sum_{n \in \mathbb{Z}} \tilde{h}_{n-2l} \sum_{m \in \mathbb{Z}} \tilde{h}_{m-2n} x_m = \langle \mathbf{x}, \tilde{\varphi}^2(\cdot - 4l) \rangle, \\ d_l^{r,2} &= \sum_{n \in \mathbb{Z}} \tilde{g}_{n-2l}^r s_n^1 = \sum_{n \in \mathbb{Z}} \tilde{g}_{n-2l}^r \sum_{m \in \mathbb{Z}} \tilde{h}_{m-2n} x_m = \langle \mathbf{x}, \tilde{\psi}^{r,2}(\cdot - 4l) \rangle, \\ \text{where } \tilde{\varphi}^2(l) &\triangleq 2 \sum_{n \in \mathbb{Z}} \tilde{h}_n \tilde{\varphi}^1(n - 2l), \quad \tilde{\psi}^{r,2}(l) \triangleq 2 \sum_{n \in \mathbb{Z}} \tilde{g}_n^r \tilde{\varphi}^1(n - 2l). \end{aligned}$$

Then, the signal \mathbf{s}^1 is restored as

$$s_l^1 = \frac{1}{2} \sum_{n \in \mathbb{Z}} h_{l-2n} s_n^2 + \frac{1}{2} \sum_{r=1}^2 \sum_{n \in \mathbb{Z}} g_{l-2n}^r d_n^{r,1}$$

and the signal \mathbf{x} is expanded into the following sums:

$$\begin{aligned} \mathbf{x} &= \frac{1}{4} \sum_{l \in \mathbb{Z}} \langle \mathbf{x}, \tilde{\varphi}^2(\cdot - 4l) \rangle \varphi^2(\cdot - 4l) + \frac{1}{4} \sum_{r=1}^2 \sum_{l \in \mathbb{Z}} \langle \mathbf{x}, \tilde{\psi}^{r,2}(\cdot - 4l) \rangle \psi^{r,2}(\cdot - 4l) \\ &+ \frac{1}{2} \sum_{r=1}^2 \sum_{l \in \mathbb{Z}} \langle \mathbf{x}, \tilde{\psi}_r^1(\cdot - 2l) \rangle \psi^{r,1}(\cdot - 2l), \\ \text{where } \varphi^2(l) &\triangleq 2 \sum_{n \in \mathbb{Z}} h_n \varphi^1(n - 2l), \quad \psi^{r,2}(l) \triangleq 2 \sum_{n \in \mathbb{Z}} g_n^r \varphi^1(n - 2l), \quad r = 1, 2. \end{aligned}$$

Thus, if condition (2.4) is satisfied then the sets of four-sample shifts of the signals $\tilde{\varphi}^2$, $\tilde{\psi}^{r,2}$, φ^2 , $\psi^{r,2}$, $r = 1, 2$ (which we call the discrete-time framelets of the second decomposition scale) and the two-sample shifts of the framelets $\tilde{\psi}^{r,1}$, $\psi^{r,1}$, $r = 1, 2$ form a new bi-frame of the signal space.

Successive iterations lead to the following expansion of the signal \mathbf{x} for $r = 1, 2$:

$$\mathbf{x} = 2^{-M} \sum_{l \in \mathbb{Z}} s_l^M \varphi^M(\cdot - 2^M l) + \sum_{r=1}^2 \sum_{\nu=1}^M 2^{-\nu} \sum_{l \in \mathbb{Z}} d_l^{r,\nu} \psi^{r,\nu}(\cdot - 2^\nu l),$$

where $s^M \triangleq \langle \mathbf{x}, \tilde{\varphi}^M(\cdot - 2^M l) \rangle$, $d^{r,\nu} \triangleq \langle \mathbf{x}, \tilde{\psi}^{r,\nu}(\cdot - 2^\nu l) \rangle$,

$$\tilde{\varphi}^M(l) \triangleq 2 \sum_{n \in \mathbb{Z}} h_n \tilde{\varphi}^{M-1}(n - 2l), \quad \tilde{\psi}^{r,\nu}(l) \triangleq 2 \sum_{n \in \mathbb{Z}} g_n^r \tilde{\varphi}^{\nu-1}(n - 2l),$$

$$\varphi^M(l) \triangleq 2 \sum_{n \in \mathbb{Z}} h_n \varphi^{M-1}(n - 2l), \quad \psi^{r,\nu}(l) \triangleq 2 \sum_{n \in \mathbb{Z}} g_n^r \varphi^{\nu-1}(n - 2l).$$

Thus, we have a new bi-frame that consists of shifts of the framelets $\tilde{\varphi}^M$, $\tilde{\psi}^{r,\nu}$ and φ^M , $\psi^{r,\nu}$, $r = 1, 2$, $\nu = 1, \dots, M$. The diagram in Figure 1 illustrates the multiscale frame transform with three-channel filter bank. Each decomposition level introduces 50% redundancy.

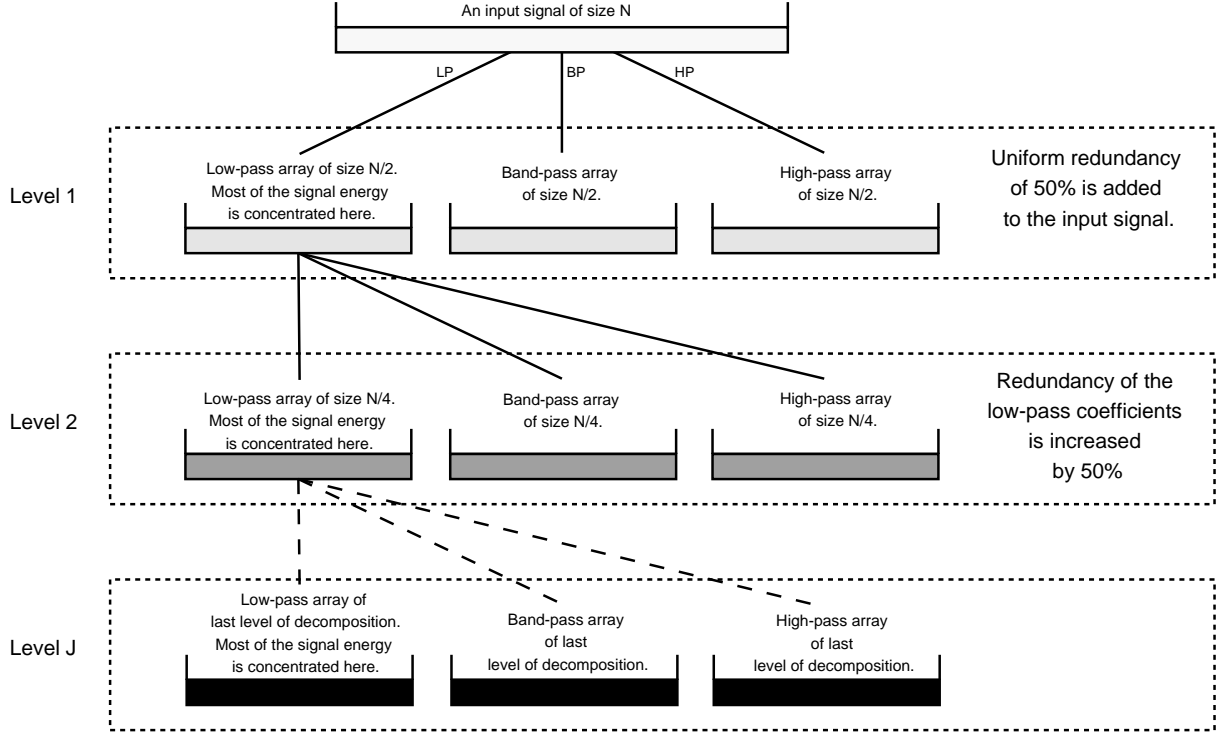


Figure 1: Diagram of multiscale frame transform with three-channel filter bank.

Under some mild conditions the low-pass filters $\tilde{H}(z)$ and $H(z)$ generate scaling functions $\tilde{\varphi}(t)$ and $\varphi(t)$ ([9]). Then continuous framelets are found from the equations

$$\tilde{\psi}^r(t) \triangleq 2 \sum_{k \in \mathbb{Z}} \tilde{g}_k^r \tilde{\varphi}(2t - k), \quad \psi^r(t) \triangleq 2 \sum_{k \in \mathbb{Z}} g_k^r \varphi(2t - k), \quad r = 1, 2, \quad (2.6)$$

Definition 2.3 *It is said that a continuous framelet ψ has m vanishing moments if $\int_{-\infty}^{\infty} \psi(t) t^r dt = 0$, $k = 0, \dots, m - 1$.*

Due to Eq. (2.6), if the framelet ψ is generated by a high-pass filter $G(z)$ then the number of its vanishing moments is equal to the multiplicity of zero of the function $G(z)$ at $z = 1$.

2.3 Interpolatory frames

Assume that the even polyphase component $F_e(z)$ of a filter $F(z)$ is $1/2$. Then, the filter is called interpolatory. In the rest of the paper we deal exclusively with filter banks, whose low-pass filters are interpolatory:

$$H(z) = \frac{1 + z^{-1}U(z^2)}{2}, \quad \tilde{H}(z) = \frac{1 + z^{-1}\tilde{U}(z^2)}{2}. \quad (2.7)$$

We assume that $U(z)$ and $\tilde{U}(z)$ are rational functions that have no poles on the unit circle $|z| = 1$, $U(1) = \tilde{U}(1) = 1$ and the following symmetry conditions hold

$$z^{-1}U(z^2) = zU(z^{-2}), \quad z^{-1}\tilde{U}(z^2) = z\tilde{U}(z^{-2}). \quad (2.8)$$

The polyphase matrices for a filter bank that use the interpolatory low-pass filters $H(z)$ and $\tilde{H}(z)$ are

$$\tilde{\mathbf{P}}(z) \triangleq \begin{pmatrix} 1/2 & \tilde{U}(z)/2 \\ \tilde{G}_e^1(z) & \tilde{G}_o^1(z) \\ \tilde{G}_e^2(z) & \tilde{G}_o^2(z) \end{pmatrix}, \quad \mathbf{P}(z) \triangleq \begin{pmatrix} 1/2 & G_e^1(z) & G_e^2(z) \\ U(z)/2 & G_o^1(z) & G_o^2(z) \end{pmatrix}.$$

Then, the perfect reconstruction condition (2.4) leads to

$$\mathbf{P}_g(z) \cdot \tilde{\mathbf{P}}_g(1/z) = \mathbf{Q}(z), \quad (2.9)$$

where

$$\begin{aligned} \tilde{\mathbf{P}}_g(z) &\triangleq \begin{pmatrix} \tilde{G}_e^1(z) & \tilde{G}_o^1(z) \\ \tilde{G}_e^2(z) & \tilde{G}_o^2(z) \end{pmatrix}, \quad \mathbf{P}_g(z) \triangleq \begin{pmatrix} G_e^1(z) & G_e^2(z) \\ G_o^1(z) & G_o^2(z) \end{pmatrix}, \\ \mathbf{Q}(z) &\triangleq \begin{pmatrix} 1/4 & -\tilde{U}(z^{-1})/4 \\ -U(z)/4 & (2 - U(z)\tilde{U}(z^{-1}))/4 \end{pmatrix}. \end{aligned}$$

We can immediately obtain a solution to (2.9) with the interpolatory filters $G^1(z)$ and $\tilde{G}^1(z)$:

$$G_e^1(z) = \tilde{G}_e^1(z) = \frac{1}{2}, \quad \tilde{G}_o^1(z) = -\frac{\tilde{U}(z)}{2}, \quad G_o^1(z) = -\frac{U(z)}{2}, \quad G_e^2(z) = \tilde{G}_e^2(z) = 0.$$

The odd components of the filters $G^2(z)$ and $\tilde{G}^2(z)$ are derived from the factorization

$$v(z)\tilde{v}(z^{-1}) = V(z), \quad \text{where } V(z) \triangleq \frac{1 - U(z)\tilde{U}(z^{-1})}{2} \quad (2.10)$$

and the filters

$$G^2(z) = z^{-1}v(z^2), \quad \tilde{G}^2(z) = z^{-1}\tilde{v}(z^2). \quad (2.11)$$

Note that the filters

$$G^1(z) = \frac{1 - z^{-1}U(z^2)}{2} = H(-z), \quad \tilde{G}^1 = \frac{1 - z^{-1}\tilde{U}(z^2)}{2} = \tilde{H}(-z) \quad (2.12)$$

are interpolatory. They are high-pass filters because $U(1) = \tilde{U}(1) = 1$. The transfer functions $G^1(z)$ and $\tilde{G}^1(z)$ are invariant about the inversion $z \rightarrow z^{-1}$ due to Eq. (2.8).

The rational function $V(z^2)$ can be written as $V(z^2) = \left(1 - z^{-1}U(z^2) \cdot z\tilde{U}(z^{-2})\right)/2 = V(z^{-2})$. Thus, a rational symmetric or antisymmetric factorization is possible. The trivial rational symmetric factorizations are $v(z) = 1, \tilde{v}(z) = V(z)$ or $\tilde{v}(z) = 1, v(z) = V(z)$. Since $V(1) = 0$, at least either the filters $G^2(z)$ or \tilde{G}^2 is high-pass.

2.3.1 Tight frames

If $U(z) = \tilde{U}(z)$ then we get $H(z) = \tilde{H}(z), G^1(z) = \tilde{G}^1(z)$ and

$$V(z) = (1 - |U(z)|^2)/2, \quad V(z^2) = 2H(z)H(-z). \quad (2.13)$$

If the inequality $|U(z)| \leq 1$ holds on the unite circle $|z| = 1$, then, the function $V(z)$ can be factored as $V(z) = v(z)v(1/z)$. Then, we have $G^2(z) = \tilde{G}^2(z)$. Thus, the synthesis filter bank coincides with the analysis filter bank and generates a tight frame.

2.3.2 Low-pass and high-pass filters

In this section we introduce a family of filters related to the widely used Butterworth filters. Let $\rho(z) \triangleq z + 2 + z^{-1}$. Thus $\rho(-z) = -z + 2 - z^{-1}$. Let

$$U^{2r}(z^2) \triangleq z \frac{\rho(z)^r - \rho(-z)^r}{\rho(z)^r + \rho(-z)^r}, \quad \chi^{2r}(z) \triangleq \frac{1}{2} (1 + z^{-1}U^{2r}(z^2)) \quad r \in \mathbb{N}. \quad (2.14)$$

These filters can serve as a source for frame constructions.

Proposition 2.1 ([4]) *The rational functions $U^{2r}(z)$, defined in (2.14), have no poles on the unit circle $|z| = 1$ and*

$$|U^{2r}(z)| \leq 1, \quad \text{as } |z| = 1 \text{ and } U^{2r}(1) = 1. \quad (2.15)$$

The symmetry condition $z^{-1}U^{2r}(z^2) = zU^{2r}(z^{-2})$ holds. The function $\chi^{2r}(z)$ has a root of multiplicity $2r$ at $z = -1$.

Remark. The functions $\chi^{2r}(z)$ and $\chi^{2r}(-z)$ coincide with the squared magnitudes of the frequency response of the low- and high-pass half-band digital Butterworth filters of order r , respectively. For details see [27, 18, 2].

2.4 Butterworth frames

The above considerations suggest that the filters $U^{2r}(z)$ and $\chi^{2r}(z)$ can be useful for the construction of frames in signal space. For this purpose, we design perfect reconstruction filter banks according to the scheme in Section 2.3. To be specific, we choose $U(z) = U^{2r}(z)$, $H(z) = \chi^{2r}(z)$, $\tilde{U}(z) = U^{2p}(z)$ and $\tilde{H}(z) = \chi^{2p}(z)$ where r and p are some natural numbers that may be equal to each other. Since there is a relation between the filters and the Butterworth filters we call the corresponding frames the Butterworth frames.

2.4.1 Tight frames

We define the filters

$$\begin{aligned} H(z) &= \tilde{H}(z) \triangleq \chi^{2r}(z) = \frac{\rho^r(z)}{\rho^r(z) + \rho^r(-z)}, \\ G^1(z) &= \tilde{G}^1(z) \triangleq \chi^{2r}(-z) = \frac{\rho^r(-z)}{\rho^r(z) + \rho^r(-z)}. \end{aligned}$$

We get a tight frame when we factorize $V^{2r}(z)$ to be $V^{2r}(z) = (1 - |U^{2r}(z)|^2) / 2 = v^r(z)v^r(1/z)$. It is always possible due to the property (2.15) of the function U^{2r} . From (2.13) we have

$$V^{2r}(z^2) = \frac{2(-1)^r z^{-2r} (1 - z^2)^{2r}}{(\rho^r(z) + \rho^r(-z))^2} \Rightarrow v^r(z^2) = \frac{\sqrt{2} (1 - z^2)^r}{\rho^r(z) + \rho^r(-z)}.$$

If $r = 2n$ then we can define $v^r(z^2)$ differently:

$$v^r(z^2) \triangleq \frac{\sqrt{2} (z - z^{-1})^{2n}}{\rho^{2n}(z) + \rho^{2n}(-z)}.$$

Hence, the three filters $H(z) = \chi^{2r}(z)$, $G^1(z) = H(-z) = \chi^{2r}(-z)$ and $G^2(z) \triangleq z^{-1}v^r(z^2)$ generate a tight frame in signal space. The discrete framelets φ^ν and $\psi^{1,\nu}$ are symmetric, whereas the framelet $\psi^{2,\nu}$ is symmetric when r is even and antisymmetric when r is odd. The frequency response of the filter $H(z)$ is maximally flat. The frequency response of the filter $G^1(z)$ is a mirrored version of $H(z)$. The frequency response of the filter $G^2(z)$ is symmetric about $\omega = \pi/2$ and it vanishes at the points $\omega = 0$ and $\omega = \pi$. Thus, $H(z)$ is a low-pass filter, $G^1(z)$ is a high-pass filter and $G^2(z)$ is a band-pass filter.

Examples

The simplest case, $r = 1$:

$$H(z) = \frac{z^{-1} + 2 + z}{4}, \quad G^1(z) = H(-z), \quad G^2(z) = \frac{\sqrt{2}(1 - z^2)}{4z}. \quad (2.16)$$

All the filters are FIR and, therefore, all the discrete framelets have finite support. This filter bank generates a tight frame in the space of square integrable functions L^2 ([32]). The framelets are piece-wise linear. The framelet ψ^1 is symmetric and has two vanishing moments, while ψ^2 is antisymmetric and has only one vanishing moment.

Case $r = 2$:

$$H(z) = \frac{(z + 2 + z^{-1})^2}{2(z^{-2} + 6 + z^2)} \quad G^1(z) = H(-z), \quad G^2(z) = \frac{\sqrt{2}z^{-1}(z - z^{-1})^2}{2(z^{-2} + 6 + z^2)}. \quad (2.17)$$

All the filters are IIR and, therefore, all the framelets have infinite support. The framelet ψ^2 is symmetric and has two vanishing moments. The framelet ψ^1 has four vanishing moments.

Remark: In [30], a parameterized family of low-pass filters was presented, which can serve as a base for the construction of a symmetric tight wavelet frame with two generators. The filter $H(z)$ is a special case of this family when $a = -1/16$.

Case $r = 3$:

$$H(z) = \frac{(z^{-1} + 2 + z)^3}{2(6z^2 + 20 + 6z^{-2})}, \quad G^1(z) = H(-z), \quad G^2(z) = \frac{\sqrt{2}z^{-1}(1 - z^2)^3}{2(6z^2 + 20 + 6z^{-2})}. \quad (2.18)$$

All the filters are IIR and, therefore, all the discrete framelets have infinite support. The framelet ψ^2 is antisymmetric and have three vanishing moments. The framelet ψ^1 has six vanishing moments. We display the frequency response of the filters and their corresponding waveforms in Fig. 2. It is seen that the waveforms are well localized in time domain. The frequency response of the filters $H(z)$ and $G^1(z)$ are mirrored versions of each other. They are maximally flat.

2.4.2 Bi-frames

Let $U(z) = U^{2r}(z)$, $\tilde{U}(z) = U^{2p}(z)$, $p, r \in \mathbb{N}$. Then, we have

$$\begin{aligned} H(z) &\triangleq \frac{\rho^r(z)}{\rho^r(z) + \rho^r(-z)} = G^1(-z), & \tilde{H}(z) &\triangleq \frac{\rho^p(z)}{\rho^p(z) + \rho^p(-z)} = \tilde{G}^1(-z), \\ G^2(z) &\triangleq z^{-1}v(z^2), & \tilde{G}^2(z) &\triangleq z^{-1}\tilde{v}(z^2). \end{aligned}$$

where $v(z^2)\tilde{v}(z^{-2}) = 1 - U^{2r}(z^2)U^{2p}(z^{-2})$. Assume $p < r$. Then, we have

$$v(z^2)\tilde{v}(z^{-2}) = \frac{(-1)^p (z - z^{-1})^{2p} (\rho^{r-p}(z) + \rho^{r-p}(-z))}{(\rho^r(z) + \rho^r(-z)) (\rho^p(z) + \rho^p(-z))}.$$

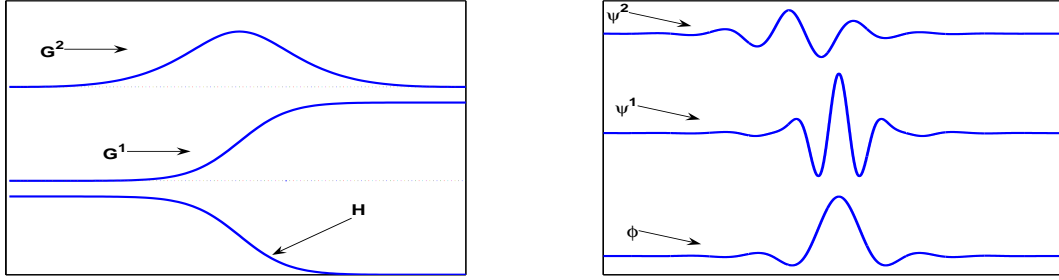


Figure 2: Tight frame that originates from the filter bank (2.18): right: waveforms, left: frequency response of the filters.

One way to (anti)symmetrically factorize this function is

$$v(z^2) = \frac{(1 - z^2)^p (\rho^{r-p}(z) + \rho^{r-p}(-z))}{\rho^p(z) + \rho^p(-z)}, \quad \tilde{v}(z^2) = \frac{(1 - z^2)^p}{\rho^r(z) + \rho^r(-z)}.$$

If $p = 2n$ then we have a symmetric factorization such as

$$v(z^2) = \frac{(z - z^{-1})^{2n} (\rho^{r-p}(z) + \rho^{r-p}(-z))}{\rho^p(z) + \rho^p(-z)}, \quad \tilde{v}(z^2) = \frac{(z - z^{-1})^{2n}}{\rho^r(z) + \rho^r(-z)}.$$

Example: Assume $p = 2$, $r = 1$.

$$\begin{aligned} H(z) &= (z^{-1} + 2 + z) / 4 = G^1(-z), & \tilde{H}(z) &= \frac{(z + 2 + z^{-1})^2}{2(z^{-2} + 6 + z^2)} = \tilde{G}^1(-z), \\ G^2(z) &= (z^{-1} - z) / 2, & \tilde{G}^2(z) &= \frac{z^{-1} - z}{z^{-2} + 6 + z^2}. \end{aligned} \quad (2.19)$$

All the synthesis filters are FIR. Consequently, the synthesis scaling function φ and the framelets ψ^1 and ψ^2 are compactly supported, unlike the analysis framelets. The synthesis and the analysis framelets ψ^2 and $\tilde{\psi}^2$ are antisymmetric and have one vanishing moment each. The synthesis framelet ψ^1 has two vanishing moments, the analysis framelet $\tilde{\psi}^1$ has four vanishing moments.

3 Erasure recovery algorithms based on framelets

The proposed framelet transform can be effectively employed as a true combined source-channel coding scheme - there is no separate source coding followed by channel coding. In fact, no explicit channel coding is used. The proposed approach makes use of naturally occurring redundancy within multilevel decomposition of framelet transforms to provide unequal error protection (UEP). The number of losses that can be sustained is only marginally image dependant.

3.1 Remarks on unequal error protection (UEP)

The multilevel framelet transform is demonstrated schematically in Figure 1. Assume that there are four levels of decomposition.

Figure 3 displays spectra of the discrete-time framelets $\psi^{r,1}$, $\psi^{r,2}$, $r = 1, 2, 3, 4$, and φ^4 that originate from the filter bank (2.18). The shifts of these framelets provide a four-level tight frame expansion of the signal. First level of decomposition produces three blocks of coefficients: low-pass, band-pass and

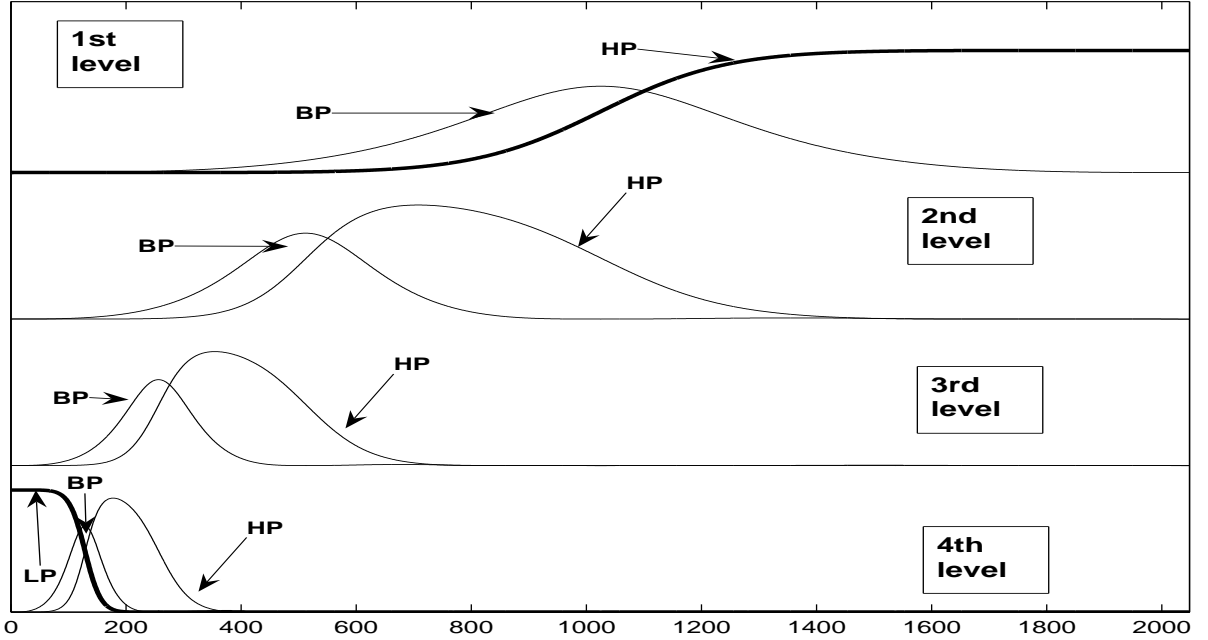


Figure 3: Spectra of the discrete-time framelets $\psi^{r,1}$, $\psi^{r,2}$, $r = 1, 2, 3, 4$, and φ^4 that originate from the filter bank (2.18). The abbreviation LP means low-pass. It is related to φ^4 , HP – high-pass – is related to $\psi^{r,1}$, BP – band-pass – is related to $\psi^{r,2}$.

high-pass. As it was explained in Section 2.2, these are the coefficients of the orthogonal projections of the signal onto the subspaces spanned by two-sample shifts of the discrete-time framelets $\varphi^1(k)$, $\psi^{1,2}(k)$ and $\psi^{1,1}(k)$, respectively. The spectra of the framelets $\psi^{1,2}(k)$ and $\psi^{1,1}(k)$ are displayed in the top row of Fig. 3. The second step of the decomposition transforms the low-pass block into three blocks of coefficients, which are the coefficients of the orthogonal projections of the signal onto the subspaces spanned by four-sample shifts of the framelets $\varphi^2(k)$, $\psi^{2,2}(k)$ and $\psi^{2,1}(k)$. The spectra of the framelets $\psi^{2,2}(k)$ and $\psi^{2,1}(k)$ are displayed in the second from the top row of the figure. The last fourth step of the decomposition transforms the low-pass block of the third level into three blocks of coefficients, which are the coefficients of the orthogonal projections of the signal onto the subspaces spanned by sixteen-sample shifts of the framelets $\varphi^4(k)$, $\psi^{4,2}(k)$ and $\psi^{4,1}(k)$. The spectra of these framelets are

displayed in the bottom row of the figure. The reconstruction consists of the synthesis of the original signal from the above set of projections.

One can see that the spectra displayed in the figure form at least two-fold cover of the frequency domain of the signal except for the frequency bands occupied by the spectra of the low-frequency framelet φ^4 and the high-frequency framelet $\psi^{1,1}$. They are highlighted by the boldface in the figure. It means that, once a projection (except for the projections on φ^4 and $\psi^{1,1}$) is lost, it can be restored from the remaining projections. Also two or more projections, whose spectra do not overlap, can be restored. In other words, erasure of a number of coefficients, from a block, or even the whole block (except for the blocks related to φ^4 and $\psi^{1,1}$) can be compensated by the coefficients from the remaining blocks.

Two exclusive blocks of coefficients related to φ^4 and $\psi^{1,1}$ must be additionally protected. The low-pass block is the most significant. Erasure of even one coefficient can essentially distort the signal. But for the four-level transform it comprises only $N/16$ coefficients, where N is the length of the signal. If we expand the transform to level J then the last low-pass block comprises only $N/2^J$ coefficients. This relatively small number of coefficients can be protected at a low computational cost.

The high-pass block related to $\psi^{1,1}$ is most populated ($N/2$ coefficients). But, due to the vanishing moments of the framelets $\psi^{1,1}$, this block contains relatively small number of significant coefficients, which correspond to sharp transients in the signal (edges in the image). Only these significant coefficients deserve an additional protection.

3.2 Channel models

A communication channel is referred to as *erasure channel* in the following cases: 1. when some of the transmitted data is simply not received (or not received on time); 2. if the channel inserts random errors whose locations are known, and the receiver chooses to treat these errors as erasures. The second case is motivated by the following: a code can typically recover from $d - 1$ erasures, but only $\frac{d}{2}$ errors, where the integer d denotes the minimum Hamming distance of the code. Two erasure channels are schematically depicted in Fig. 4.

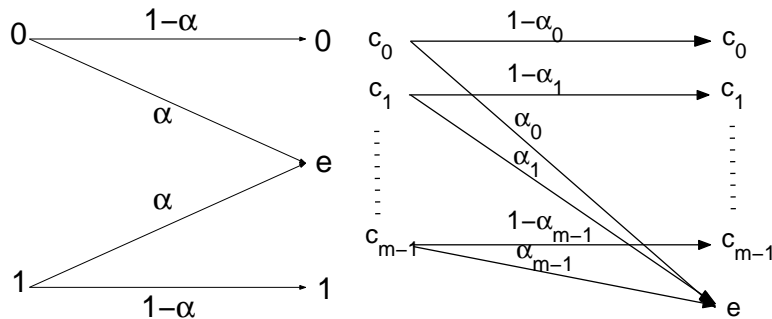


Figure 4: **a.** Binary erasure channel. **b.** General erasure channel.

In general, an erasure channel has an input alphabet of cardinality m with $m + 1$ outputs, where α_i is the probability of symbol C_i being erased. In the following it will be assumed that all probabilities α_i are equal. For $m = 2$, this channel reduces to the well known binary erasure channel (BEC). The BEC has two inputs and three outputs with probability of erasure α . In the current work, random erasure of complete coefficients, corresponding to the channel model of Fig. 4.b, will be discussed. (In this model, the erased coefficients may be considered as being in error.)

3.3 Algorithms for error recovery

3.3.1 Encoding a source image

When a source image is encoded, a 2-D array of framelet transform is generated in the following way. First, bandpass, low-pass and high-pass filters, denoted B, L and H, respectively, are applied to the rows of the image. The columns of the resulting output are then processed using the same set of filters. Consequently, nine bands are obtained: BB, BL, BH, LB, LL, LH, HB HL and HH. The band LL, which corresponds to the most important (low frequency) information, is then processed in the same way to obtain the second level in the decomposition. This process is repeated recursively until the desired level of decomposition is reached. In Section 3.3.2 we describe a framelet-based algorithm that recovers from erasures of whole transform coefficients.

Some notation are required prior to the algorithm description. Assume that the original 2D image is arranged into a 1D array $X \in \mathbb{R}^N$ and the coefficients of its 2D framelet transform are arranged into a 1D array $Y \in \mathbb{H} \subset \mathbb{R}^K$ of length $K > N$. Let $\mathcal{S} \triangleq \{C_k\}_1^{nm}$ be the set of coordinates of this array, and let $E \subset \mathcal{S}$ be the set of coordinates of the erased coefficients. The subspace $\mathbb{H} \subset \mathbb{R}^K$ is called the space of codewords. Define $\bar{E} \triangleq \mathcal{S} \setminus E$ and \tilde{Y} is obtained from Y by erasing all coefficients that correspond to E . Let \tilde{F} be the analysis operator $\tilde{F} : \mathbb{R}^N \mapsto H \subset \mathbb{R}^K, K > N$ associated with the framelet transform: $Y = \tilde{F} X$. Obviously, $rank(\tilde{F}) = N$. Let F be the inverse operator (i.e. the synthesis operator) of \tilde{F} . We denote by $\hat{\tilde{F}}$ the matrix \tilde{F} with erased rows determined by the coordinates of E . Assume that \tilde{Y} contains zeros instead of all substitute zeros for all erased coefficients in \tilde{Y} . erased coefficients. If $rank(\hat{\tilde{F}}) = N$, then \tilde{Y} contains sufficient information to recover the original data X .

3.3.2 Recovery of the Coefficient Erasures (CCE)

Each coefficient of a transformed image is presented by a few bits. If one, or more bits associated with the same coefficient are lost in transit, the whole coefficient may be treated as an erasure, or alternatively, as being in error. It is well known that, in general, recovering from erasures is easier than recovering from errors. Hence, the motivation for the algorithm. This algorithm is a slightly modified version of the well-known Gerchberg [12]– Papoulis [28] algorithm. The Gerchberg – Papoulis

algorithm was applied, in particular, to interpolation of data given on an irregular grid. The application of the mentioned algorithm to the erasure recovery had been reported by Petukhov at the Fifth AFA Conference on Curves and Surfaces, Saint Malo, 2002.

It utilizes the redundancy inherent in frame transforms to recover from erasures of whole coefficients that occur during transmission. The appropriate channel model in this case is the general erasure channel (GEC).

As before, \tilde{Y} denotes the received set of coefficients with the convention that erased coefficients are substituted by zeros. Let y^k denote the set of (received+recovered) framelet coefficients at iteration k of the recovery algorithm. Assume the image intensities belong to the interval $[L_0, L_{255}]$, where $L_0 < L_{255}$.

Initialize $y^{(0)} = \tilde{Y}$;

for $k = 0$ *to* $K - 1$

$\hat{x}^{(k)} = Fy^{(k)}$; *fit out-of-interval values into* $[L_0, L_{255}]$;

$\hat{y}^{(k)} = \tilde{F}^* \hat{x}^{(k)}$;

$y^{(k+1)} = \hat{y}^{(k)}$ *on the coordinates of* E ;

$y^{(k+1)} = \tilde{Y}$ *on the coordinates of* \bar{E} ;

end.

This framelet-based algorithm iteratively recovers an image from its transformed version \tilde{Y} that contains erasures. The recovered image at each iteration is given by $\hat{x}^{(k)}$. The convergence properties of the proposed algorithm are discussed next. Assume having a three-channel filter bank implements a framelet transform of the vector $x = (x_1, x_2)$. Denote by $\{x_{\psi^i}\}_{i=1}^3$ the framelet representation of x . Clearly, $\mathcal{S} = \{1, 2, 3\}$, and we further assume that $e \in \mathcal{S}$ is an index of erasure (e.g. $e = 2$). The algorithm first sets the erased coefficient to zero. Then, it reconstructs the image from its corrupt set of framelet coefficients. This operation may result in an erroneous estimate of x ; the estimation of x at iteration k may be written as $\hat{x}^{(k)} = x + \varepsilon^{(k)}$, where ε denotes the reconstruction error. In practice, the intensities of an image are confined to $[L_0, L_{255}]$; thus, if $\hat{x}^{(k)}$ is out-of-interval, it can immediately fit back. Experimental results show that this approach typically accelerates the convergence of the algorithm, however, it does not improve the correction capability. This acceleration is the result of a correction made in the image domain. The reconstructed image $\hat{x}^{(k)}$ is then decomposed (again) to provide $\hat{y}^{(k)}$, thus spreading the error ε over all three framelet elements. The correct values of the elements $\{x_{\psi^i}\}_{i \in \{1, 2, 3\} \setminus e}$, are actually known from \tilde{Y} , and are therefore reassigned. Since the redundancy ratio of the proposed wavelet approach is less than one ($R = 2/3$), the residual error after reassignment is decreasing exponentially in the number of iterations k . This assertion can be

justified as follows. Denote the framelet elements of the three-channel filter bank by $\{\psi^i\}_{i=1}^3$ and denote $\hat{y}^{(0)} \triangleq \langle \psi^i, x \rangle_{i \in \{1,2,3\} \setminus e} \triangleq \{x_{\psi^i}\}_{i \in \{1,2,3\} \setminus e}$; then, by following the above notation we can write,

$$\begin{aligned} \hat{x}^{(k)} &= R \sum_{i=1}^3 \hat{y}^{(k-1)} \psi^i = R \sum_{i \in \{1,2,3\} \setminus e} \langle \psi^i, x \rangle \psi^i + R \langle \psi^e, \hat{x}^{(k-1)} \rangle \psi^e \\ &= R \sum_{i \in \{1,2,3\} \setminus e} \langle \psi^i, x \rangle \psi^i + R \langle \psi^e, x + \varepsilon^{(k-1)} \rangle \psi^e \\ &= R \underbrace{\sum_{i \in \{1,2,3\} \setminus e} \langle \psi^i, x \rangle \psi^i}_x + R \langle \psi^e, x \rangle \psi^e + R \langle \psi^e, \varepsilon^{(k-1)} \rangle \psi^e. \end{aligned}$$

Thus, we have $\hat{x}^{(k)} = x + R \langle \psi^e, \varepsilon^{(k-1)} \rangle \psi^e = x + \varepsilon^{(k)}$ where $\varepsilon^{(k)} = R \langle \psi^e, \varepsilon^{(k-1)} \rangle \psi^e$. Recursively, we get

$$\hat{x}^{(k)} = x + R \langle \psi^e, \varepsilon^{(k-1)} \rangle \psi^e = x + R \langle \psi^e, R \langle \psi^e, \varepsilon^{(k-2)} \rangle \psi^e \rangle \psi^e = \dots = x + R^k \varepsilon \psi^e.$$

The above derivation is motivated by the following argument. Since reconstruction of an image (see Eq. (2.3) and the above analysis) is a linear process, and due to the exponential decay (locality) of the framelet elements, the convergence rate of a signal, which contains a large number of errors, is closely approximated by that of a single coefficient.

Finally, we note that the filter banks introduced in Section 2 consist of IIR filters with rational transfer functions. Filtering can be implemented in a fast recursive mode. Thus, the complexity of the transform is proportional to N operations, where N is the number of pixels in the original image. The inherent unequal error protection properties of the framelet representation makes this approach a most natural candidate for the task of protecting image transfer over an erasure channel. But can this approach match up to classical coding techniques - this is the topic of Section 4.

4 The Framelet transform and classical error correcting coding

Through the years many error correcting codes and decoding algorithms have been designed to protect data transmission through imperfect channels. Information theory, established by Shannon [34], and coding theory provide theoretic bounds on the rate of information that can be reliably transmitted through a given channel.

Comparing between the error recovery capabilities of the proposed framelet transform and classical error correcting codes is not a straightforward task. This is due to the nature of digital representation of images, i.e. the fact that the source data is not equally significant. The framelet transform, as employed in this paper, may, of course, be regarded as a redundant representation. It is based on the fact that the source is not "white", i.e., typically, the low frequencies contain more energy than the higher frequencies. It is therefore not suitable for compressed images. Bearing this in mind, we

shall now try to show, primarily by means of examples, that the framelet transform is an interesting alternative to classical source-channel coding for image transfer over noisy channels.

4.1 Comparison

A *Linear-Code* \mathcal{C} over a finite field \mathbb{F}_q of order q is defined by the triplet $[n, k, d]$, where n is the length of the code, k is the size of the source signal and d is the minimum Hamming distance of the code. It is well known that a code of minimum distance d is capable of recovering from $d - 1$ or fewer erasures. Thus, in order to perfectly recover from a portion of erasures (exactly) α , it is required that

$$d \geq \alpha n + 1. \quad (4.1)$$

Much like classical encoding schemes, the framelet transform maps a source image of dimension k_f symbols onto a framelet image of n_f symbols, where $n_f > k_f$. As an example, consider a severely degraded channel with erasure probability $\alpha = 0.6$. Simulation results (presented in Section 5) reveal that the proposed framelet-based scheme can easily reconstruct the transmitted image, with no apparent quality degradation, when as much as 60% of the data is lost in transit. According to (4.1), in order to fully recover from 60% loss, would require a classical error correcting code to have minimum distance $d = 0.6n + 1$.

Interestingly, one can hardly expect an error correcting code of length n to have the aforementioned minimum distance, and at the same time have reasonable dimension k . This assertion is easily verified by employing the Griesmer bound [14]. The Griesmer bound states that, given code parameters (k, d) , the length of a code is lower bounded by

$$n \geq g_q(k, d) \triangleq \sum_{i=0}^{(k-1)} \left\lceil \frac{d}{q^i} \right\rceil. \quad (4.2)$$

Substituting $q = 2$ and $d = 0.6n + 1$ into (4.2), we have $n \geq \sum_{i=0}^{(k-1)} \left\lceil \frac{0.6n+1}{2^i} \right\rceil$, which cannot be satisfied for any $k > 2$, since already for $k = 3$, $\left\lceil 0.6n + 1 \right\rceil + \left\lceil \frac{0.6n+1}{2} \right\rceil + \left\lceil \frac{0.6n+1}{4} \right\rceil \geq 1.05n + 1.75$.

In the examples that follow in Section 5, source image of size $k_f = 512 \times 512 = 262144$ is transformed into a framelet image of size $n_f = 697303$. Now assume a classical approach of employing compression followed by channel coding. The above derivation suggests that the source image be compressed by a factor $k_f/3 = 262144/3$, to merely 3 information symbols!, and then encoded to length $n = 697303$. Recall, however, that this extreme and unrealistic approach is required in order to *perfectly* recover from *any* portion of loss of entries of at most 0.6. Fortunately, perfect recovery of a source image is not a must. It is typically sufficient that the PSNR of the reconstructed image is high. Thus, rather than aiming at perfect recovery, one can look for a code that introduces the same amount of redundancy as

the proposed scheme and can recover from 60% loss with high probability. In terms of classical coding, the rate of the framelet transform used in our examples is given by $k_f/n_f = 0.376$. The question is whether known error correcting codes of similar rate can be considered as worthy candidates for protecting the source image. State of the art error correcting codes suitable for the BEC are the so-called low density parity check (LDPC) codes [11], and Irregular repeat-accumulate (IRA) codes [20]. In particular, Tornado codes [24], a class of LDPC codes, and the bounded-complexity IRA (BC-IRA) codes [17], are considered most efficient codes for the binary erasure channel. For example, Tornado codes possess the following property: for any given rate R and any given real number ϵ , a family of linear codes of length n and rate R can be constructed such that a codeword can be recovered with high probability from a portion $(1 + \epsilon)k$ or more of its entries. Thus, the capacity of a BEC channel, $1 - \alpha$, can be approached arbitrarily close for any erasure probability α . For the parameters of our example, $\alpha = 0.6$, $R = 0.376$, it follows that a suitable Tornado code may indeed be constructed; it should operate in the feasible region below capacity, and its gap (in rate) to capacity is easily calculated to be 0.06. In conclusion, assuming the parameters of our example are sufficiently long so that the asymptotic assumptions in [24, 17] hold, BC-IRA codes and Tornado codes should provide similar performance with similar complexity to those obtained with the framelet transform.

Finally, we note that the framelet transform, being image aware, is most tolerable to changes in channel properties. Combined with the multilevel decomposition approach described in the previous section, it exhibits graceful degradation of image quality under large dynamic changes of erasure probability. This is demonstrated in Section 5.

5 Experimental results

We conducted a series of experiments on image recovery from erasures of the transform coefficients. This can be regarded as a simulation of channels with the erasures. To be specific, we applied the framelet decomposition to the image down to the fourth level. The redundancy factor of this decomposition is 2.66. Then $\alpha \cdot 100\%$ of the transform coefficients, whose locations were randomly determined, were put to zero. We restored the images using the iterative algorithm described in Section 3.3.2. We tested two benchmark images *Barbara* and *Boats* and two biomedical images taken by MRI scanner, using $\alpha = 0.1, 0.2, 0.3, 0.4, 0.5, 0.6, 0.7$. Three different types of framelets were tested: symmetric tight framelets (Eq. (2.17)), antisymmetric tight framelets (Eq. (2.18)) and antisymmetric bi-framelets (Eq. (2.19)). The distance between the original and the restored images was evaluated via the peak signal to noise ratio (PSNR):

$$PSNR = 10 \log_{10} \left(\frac{N 255^2}{\sum_{i=1}^N (I_1(i) - I_2(i))^2} \right)$$

where I_1 and I_2 are the original image and the recovered image, respectively, and N is the number of pixels in the image.

The experimental results are summarized in Table 1 and illustrated by Fig. ???. The results for all tested images are similar to each other, therefore, for brevity, we present values of PSNR that are averaged over the four images. The results demonstrate a graceful degradation in performance when the erasure probability of the coefficients increases up to 0.7. The performance of the symmetric and antisymmetric tight frames is almost identical, while the bi-frame produces images with a slightly lower PSNR.

Erasure	10%	20%	30%	40%	50%	60%	70%
PSNR/Bi-frame	51.8418	50.7470	49.0475	46.3734	40.7849	32.3740	19.2204
PSNR/Symm.TF	52.0012	51.3969	50.0345	47.9709	43.6514	32.9655	19.7563
PSNR/Antisymm.TF	52.2622	51.3204	50.2554	48.2412	43.1816	32.8288	19.5409

Table 1. Values of the PSNR of the reconstructed images using symmetric tight frames (2.17), antisymmetric tight frames (2.18) and bi-frames (2.19). alues of the PSNR are averaged over four images.

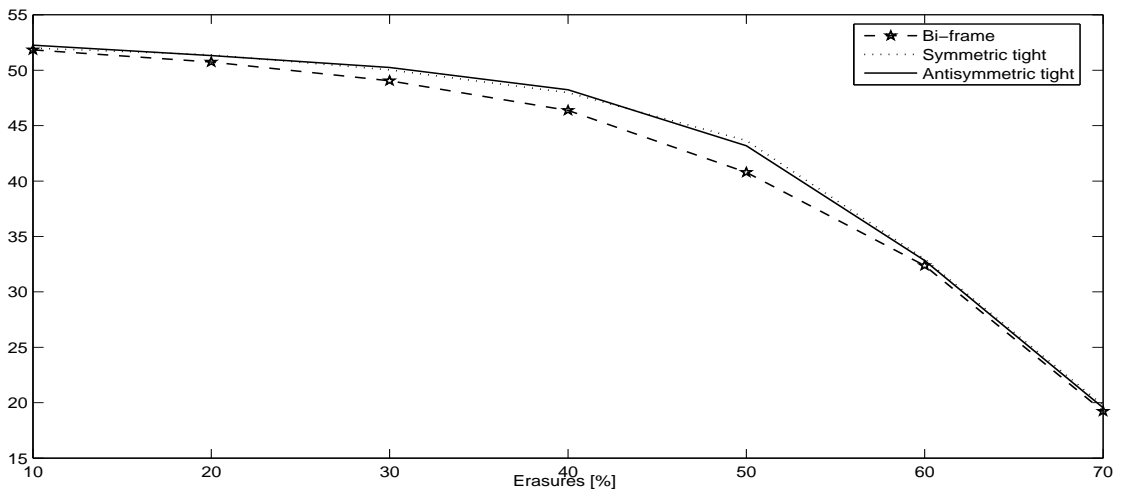


Figure 5: Averaged PSNR of the reconstructed images vs. coefficient erasure probability.

In addition, we display the results from the restoration of the four images in Figs. 6 – 9. All the figures are similarly organized. Each of them comprises three pictures. The left picture displays the original image, the central one displays the image reconstructed from the corrupted set of the transform coefficients and the right picture displays the recovered image. One can observe from the images that the restoration scheme based on the wavelet frames presented in the paper produces satisfactory output even for 60 percent of randomly erased coefficients. For 50 and, especially, for 40 percent of erased coefficients the restored images hardly can be distinguished from the original ones.



Figure 6: Results from the application of the antisymmetric tight framelet transform. Left: corrupted image with 60% erased coefficients. Right: recovered image. PSNR = 32.24.

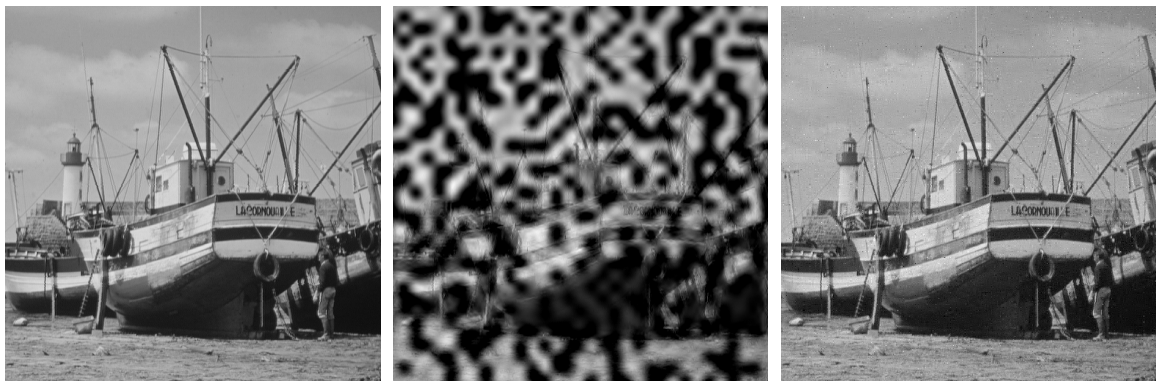


Figure 7: Results from the application of the symmetric tight framelet transform. Left: corrupted image with 60% erased coefficients. Right: recovered image. PSNR = 31.98.

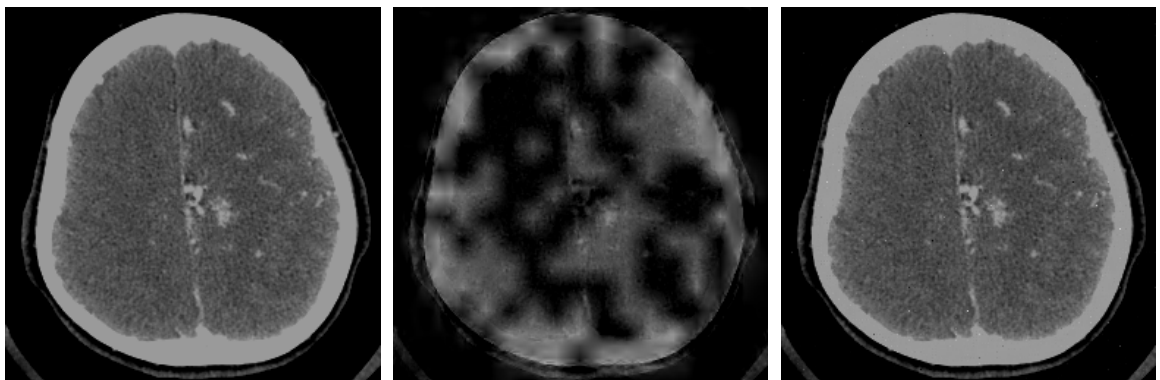


Figure 8: Results from the application of symmetric bi-framelet transform. Left: corrupted image with 50% erased coefficients. Right: recovered image. PSNR = 43,354.

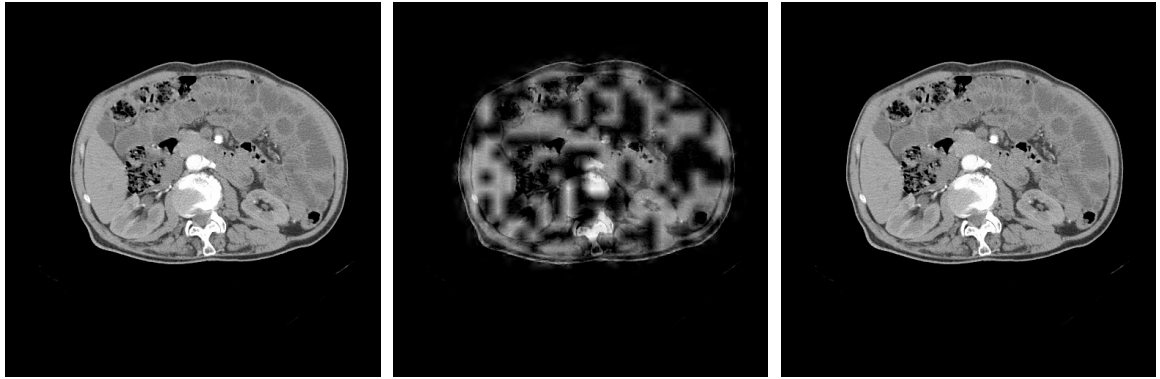


Figure 9: Results from the application of the bi-framelet transform. Left: corrupted image with 40% erased coefficients. Right: recovered image. PSNR = 52.461.

6 Conclusions

We introduced in [4, 6] new classes of tight and bi- framelets as well as multiframelets [5] that combine properties that are needed in signal processing, such as symmetry, at spectra, sufficient number of vanishing moments, interpolation and moderate redundancy, set aside an efficient implementation. Some of them are described in Section 2 and are employed to design robust erasure/error recovery algorithms (see Section 2). The proposed coding approach makes use of naturally occurring redundancy within a multilevel framelet transform to recover from coefficient losses. The number of losses that can be sustained is only marginally image dependant.

In Section 5, we demonstrate the performance of the above mentioned methods with a few examples. In these examples, we decompose several images using four levels of framelet transform. Consequently, the image coefficients were fortified with four levels of redundant decomposition - thus providing an un-equal error protection. Experimental results of the proposed algorithms demonstrate recovery of images when (as much as) 60% of the data is either lost or corrupted. The recovery properties are demonstrated for various wavelet frames. We discussed the error recovery capabilities of the proposed framelet-based algorithms in comparison with classical error correction codes.

In the experiments we compared the performance of two types of tight frames, which have different number of vanishing moments and a bi-frame. The experiments demonstrated almost identical performance of these tight frames, which is superior to the performance of the bi-frame. This is the indication that the tightness rather than the number of vanishing moments is essential for the successful recovery. But this issue deserves a thorough examination.

Due to their exclusive properties, the new families of framelet transforms may have a wide range of signal processing applications, in particular, in error protection of transmitted signals and denoising audio signals and images. Incorporating framelet representation within lossy compression schemes is

left for future study.

References

- [1] V. Zheludev A. Averbuch. Construction of biorthogonal discrete wavelet transforms using interpolatory splines. *Applied and Comp. Harmonic Analysis*, 12(12):25–56, 2002.
- [2] A. B. Pevnyi A. Z. Averbuch and V. A. Zheludev. Butterworth wavelet transforms derived from discrete interpolatory splines: Recursive implementation. *Signal Processing*, 81:2363–2382, 2001.
- [3] A. Z. Averbuch and V. A. Zheludev. A new family of spline-based biorthogonal wavelet transforms and their application to image compression. *IEEE Trans. on Image Proc.*, 13(7):993–1007, 2004.
- [4] A. Z. Averbuch, V. A. Zheludev, and T. Cohen. Interpolatory frames in signal space. *To appear in IEEE Trans. Signal Processing*.
- [5] Amir Z. Averbuch, Valery A Zheludev, and Tamir Cohen. Multiwavelet frames in signal space originated from hermite splines. *Submitted to IEEE Trans. on Signal Processing*.
- [6] Amir Z. Averbuch, Valery A Zheludev, and Tamir Cohen. Tight and sibling frames originated from discrete splines. *to appear in Signal Processing*.
- [7] Z. Cvetković and M. Vetterli. Oversampled filter banks. *IEEE Transactions on signal processing*, 46(5):1245–1255, May 1998.
- [8] H. L. Cycon D. Marpe, G. Heising and A. P. Petukhov. Video coding using a bilinear image warping motion model and wavelet-based residual coding. In *Proc. SPIE Conf. on Wavelet Applications in Signal and Image Processing VII*, volume 3813, pages 401–408. SPIE, 1999.
- [9] I. Daubechies. *Ten lectures on wavelets*. SIAM., Philadelphia, PA, 1992.
- [10] M. Kieffer P. Duhamel L. Vandendorpe F. Labeau, J. C. Chiang and B. Macq. Oversampled filterbanks as error correcting codes: theory and impulse correction. *IEEE Trans. on Signal Processing*, 53:4619–4630, December, 2005.
- [11] R. G. Gallager. Low-density parity-check codes. *IRE Trans. Information Theory*, IT-8:21–28, 1962.
- [12] R.W. Gerchberg. Super-resolution through error energy reduction. *Optica Acta*, 21(9):709–720, 1974.

- [13] V. K Goyal, J. Kovacevic, and J.A. Kelner. Quantized frame expansions with erasures. *Appl. and Comput. Harmonic Analysis*, 10(3):203–233, 2001.
- [14] J. H. Griesmer. A bound for error-correcting codes. *IBM Res. Develop.*, 4:532–542, 1960.
- [15] C. Guillemot and G. Rath. Characterization of a class of error correcting frames for robust signal transmission over wireless communication channels. *EURASIP J. on Applied Signal Processing*, 2:229–241, 2005.
- [16] F. Hlawatsch H. Bölcskei and H. G. Feichtinger. Frame-theoretic analysis of oversampled filter banks. *IEEE Transactions on signal processing*, 46(12):3256–3268, Dec 1998.
- [17] I. Sason H. D. Pfister and R. Urbanke. Capacity-achieving ensembles for the binary erasure channel with bounded complexity. *to appear in IEEE Trans. on Information Theory*.
- [18] C. Herley and M. Vetterli. Wavelets and recursive filter banks. *IEEE Trans. Signal Proc.*, 41(12):2536–2556, 1993.
- [19] Q. Jiang. Parameterizations of masks for tight affine frames with two symmetric/antisymmetric generators. *Adv. Comput. Math.*, 18:247–268, February 2003.
- [20] H. Jin, A. Khandekar, and R. J. McEliece. Irregular repeat-accumulate codes. In *Proc. of the Second International Symposium on Turbo Codes and Related Topics*, pages 1–8, Brest, France, September 2000.
- [21] J. Kovacevic, P.L. Dragotti, and V. K Goyal. Filter bank frame expansions with erasures. *IEEE Trans. Inform*, 48(6):1439–1450, 2002.
- [22] C. Lan, T. Chu, K. R. Narayanan, and Z. Xiong. Scalable image and video transmissions using irregular repeat accumulate (ira) codes with fast algorithm for optimal unequal error protection. *IEEE Trans. Commun.*, 52:1092–1101, July 2004.
- [23] C. Lan, K. R. Narayanan, and Z. Xiong. Scalable image transmission using rate-compatible irregular repeat accumulate (ira) codes. In *Proceedings of the international conference on image processing*, volume 3, pages 717– 720. IEEE, June 2002.
- [24] M. G. Luby, M. Mitzenmacher, M. A. Shokrollahi, and D. A. Spielman. Efficient erasure correcting codes. *IEEE Trans. on Information. Theory*, IT-47:569–584, Feb 2001.
- [25] S. Marinkovic and C. Guillemot. Joint source-channel coding based on cosine-modulated filter banks for erasure-resilient signal transmission. *EURASIP J. on Applied Signal Processing*, 4:510–524, 2005.

- [26] R. Motwani and C. Guillemot. Tree structured oversampled filterbanks as joint source-channel codes: Application to image transmission over erasure channels. *IEEE Trans. on Signal Processing*, 52:2584–2599, September, 2004.
- [27] A. V. Oppenheim and R. W. Schaffer. *Discrete-time signal processing*. Englewood Cliffs, New York, Prentice Hall, 1989.
- [28] A. Papoulis. A new algorithm in spectral analysis and band-limited extrapolation. *IEEE Trans. Circuits Systems*, 22:735–742, September 2002.
- [29] A. P. Petukhov. Biorthogonal wavelet bases with rational masks and their applications. *Trudy St.Petersburg Mat. Ob.*, 7:168–193, 1999.
- [30] A. P. Petukhov. Framelets with many vanishing moments. In L.Shumaker C.Chui and J.Stöckler, editors, *Approximation Theory X: Wavelets, Splines, and Applications*, pages 425–432. Vanderbilt Univ. Press, 2002.
- [31] A. P. Petukhov. Symmetric framelets. *Constr. Approx.*, 19:309–328, 2003.
- [32] A. Ron and Z. Shen. Affine systems in $l^2(r^d)$: the analysis of the analysis operator. *Funct. Anal.*, 148:408–447, 1997.
- [33] I. W. Selesnick and A. F. Abdelnour. Symmetric wavelet tight frames with two generators. *Applied and Computational Harmonic Analysis*, 17:211–225, September 2004.
- [34] C. E. Shannon. A mathematical theory of communication. *The Bell System Technical Journal*, 27:379–423, 1948.